communications physics

ARTICLE

https://doi.org/10.1038/s42005-021-00565-9 OPEN

Temperature chaos is present in off-equilibrium spin-glass dynamics

Marco Baity-Jesi[1], Enrico Calore[2], Andrés Cruz[3,4], Luis Antonio Fernandez[5], José Miguel Gil-Narvion[4], Isidoro Gonzalez-Adalid Pemartin[5], Antonio Gordillo-Guerrero[6,7], David Iñiguez[3,4,8], Andrea Maiorano[9,10], Enzo Marinari[11,12], Víctor Martin-Mayor[5], Javier Moreno-Gordo[3,4✉], Antonio Muñoz-Sudupe[5], Denis Navarro[13], Ilaria Paga[14], Giorgio Parisi[11,12], Sergio Perez-Gaviro[3,4,15], Federico Ricci-Tersenghi[11,12], Juan Jesús Ruiz-Lorenzo[7,16], Sebastiano Fabio Schifano[17], Beatriz Seoane[5], Alfonso Tarancon[3,4], Raffaele Tripiccione[2] & David Yllanes[4,18]

Experiments featuring non-equilibrium glassy dynamics under temperature changes still await interpretation. There is a widespread feeling that temperature chaos (an extreme sensitivity of the glass to temperature changes) should play a major role but, up to now, this phenomenon has been investigated solely under equilibrium conditions. In fact, the very existence of a chaotic effect in the non-equilibrium dynamics is yet to be established. In this article, we tackle this problem through a large simulation of the 3D Edwards-Anderson model, carried out on the Janus II supercomputer. We find a dynamic effect that closely parallels equilibrium temperature chaos. This dynamic temperature-chaos effect is spatially heterogeneous to a large degree and turns out to be controlled by the spin-glass coherence length ξ. Indeed, an emerging length-scale ξ^* rules the crossover from weak (at $\xi \ll \xi^*$) to strong chaos ($\xi \gg \xi^*$). Extrapolations of ξ^* to relevant experimental conditions are provided.

[1] Eawag, Überlandstrasse 133, CH-8600 Dübendorf, Switzerland. [2] Dipartimento di Fisica e Scienze della Terra, Università di Ferrara e INFN, Sezione di Ferrara, I-44122 Ferrara, Italy. [3] Departamento de Física Teórica, Universidad de Zaragoza, 50009 Zaragoza, Spain. [4] Instituto de Biocomputación y Física de Sistemas Complejos (BIFI), 50018 Zaragoza, Spain. [5] Departamento de Física Teórica, Universidad Complutense, 28040 Madrid, Spain. [6] Departamento de Ingeniería Eléctrica, Electrónica y Automática, U. de Extremadura, 10003 Cáceres, Spain. [7] Instituto de Computación Científica Avanzada (ICCAEx), Universidad de Extremadura, 06006 Badajoz, Spain. [8] Fundación ARAID, Diputación General de Aragón, 50018 Zaragoza, Spain. [9] Dipartimento di Biotecnologie, Chimica e Farmacia, Università degli studi di Siena, 53100 Siena, Italy. [10] INFN, Sezione di Roma 1, I-00185 Rome, Italy. [11] Dipartimento di Fisica, Sapienza Università di Roma, I-00185 Rome, Italy. [12] CNR-Nanotec, Rome Unit, I-00185 Rome, Italy. [13] Departamento de Ingeniería, Electrónica y Comunicaciones and I3A, U. de Zaragoza, 50018 Zaragoza, Spain. [14] Dipartimento di Fisica, Sapienza Università di Roma, INFN, Sezione di Roma 1, I-00185 Rome, Italy. [15] Centro Universitario de la Defensa, 50090 Zaragoza, Spain. [16] Departamento de Física, Universidad de Extremadura, 06006 Badajoz, Spain. [17] Dipartimento di Scienze Chimiche e Farmaceutiche, Università di Ferrara e INFN Sezione di Ferrara, I-44122 Ferrara, Italy. [18] Chan Zuckerberg Biohub, San Francisco, CA 94158, USA. ✉email: jmorenogordo@gmail.com

An important lesson taught by spin glasses[1] regards the fragility of the glassy phase in response to perturbations such as changes in temperature—temperature chaos (TC)[2–19]—in the couplings[6,7,13,14] or in the external magnetic field[5,20,21]. In particular, it is somewhat controversial[22–27] whether or not TC is the physical mechanism underlying the spectacular rejuvenation and memory effects found in spin glasses[28–31] and several other materials[32–36]. Indeed, a major obstacle in the analysis of these non-equilibrium experiments is that TC is a theoretical notion which is solely defined in an equilibrium context.

Specifically, TC means that the spin configurations that are typical from the Boltzmann weight at temperature T_1 are very atypical at temperature T_2 (no matter how close the two temperatures T_1 and T_2 are).

This equilibrum notion of TC has turned out to be remarkably elusive, even in the context of Mean-Field models (i.e., models that can be solved exactly in the Mean-Field approximation). Indeed, establishing the existence of TC for the Sherrington-Kirkpatrick model has been a real tour de force[12]. Although Sherrington-Kirkpatrick's model is the Mean-Field model of more direct relevance for this work, let us recall for completeness that TC has been investigated as well in other Mean-Field systems named p-spin models. In these models, groups of $p \geq 3$ spins interact (instead, $p = 2$ for Sherrington-Kirkpatrick). Surprisingly enough, one finds different behaviors. On the one hand, we have a recent mathematical proof of the absence of TC in the homogeneous spherical p-spin model[37], in agreement with a previous claim based on physical arguments[38]. On the other hand, TC should be expected when one mixes several values of p[39], as confirmed by a quite recent mathematical analysis[40–43]. Unfortunately, the mathematically rigorous analysis of TC in off-equilibrium dynamics seems out of reach for now, even in the Mean-Field context.

In order to obtain experimentally relevant results, one needs to go beyond the Mean-Field approximation and study short-range spin glasses, represented by the Edwards-Anderson model[44,45]. In this case, analytical investigations are even more difficult, but the equilibrium notion of TC that we have outlined above has been studied through numerical simulations. Yet, these equilibrium simulations have been limited to small system sizes by the severe dynamic slowing down[6–8,11,13,14,16–19].

Here we tackle the problem from a different approach by showing that a non-equilibrium TC effect is indeed present in the dynamics of a large spin-glass sample in three spatial dimensions (our simulations of the Edwards-Anderson model are carried out on the Janus II custom-built supercomputer[46]). In a reincarnation of the statics-dynamics equivalence principle[47–50], just as equilibrium TC is ruled by the system size, dynamic TC is found to be governed by the time-growing spin-glass coherence length $\xi(t_w)$, where the waiting time t_w is the time elapsed since the system was suddenly quenched from some very high temperature to the working temperature T. Below the critical temperature, $T < T_c$, the spin glass is perennially out of equilibrium as evinced by the never-ending (and sluggish) growth of glassy magnetic domains of size $\xi(t_w)$, see refs. [51,52] for instance. Now, the extreme sample-to-sample variations found in small equilibrated systems[16,17,19,53–55] translate into a strong spatial heterogeneity of dynamic TC. Despite such strong fluctuations, our large-scale simulations allow us to observe traces of the effect even in averages over the whole system. In close analogy with equilibrium studies[16], however, dynamic TC can only be fully understood through a statistical analysis of the spatial heterogeneity. A crossover length ξ^* emerges such that TC becomes sizeable only when $\xi(t_w) > \xi^*$. We find that ξ^* diverges when the two observation temperatures T_1 and T_2 approach. The analysis of this divergence reveals that ξ^* is the non-equilibrium partner of the equilibrium chaotic length[3,56]. The large values of $\xi(t_w)$ that we reach with Janus II allow us to perform mild extrapolations to reach the most recent experimental regime[57].

In equilibrium, sample-averaged signals of TC become more visible when the size of the system increases[16]. Analogously, off-equilibrium a weak chaotic effect grows with $\xi(t_w)$ when the whole system is considered on average. Hoping that studying spatial heterogeneities will help us to unveil dynamic TC, we shall consider spatial regions of spherical shape and linear size $\sim \xi(t_w)$, chosen randomly within a very large spin glass. Statics-dynamics equivalence suggests regarding these spheres as the non-equilibrium analog of small equilibrated samples of linear size $\sim \xi(t_w)$. The analogy with equilibrium studies[16,17,19] suggests that a small fraction of our spheres will display strong TC. The important question will be how this rare-event phenomenon evolves as $\xi(t_w)$ grows (in equilibrium, the fraction of samples not displaying TC is expected to diminish exponentially with the number of spins contained in the sample[12,15]).

Results and discussion

Model. We simulate the standard Edwards-Anderson model in a three-dimensional cubic lattice of linear size $L = 160$ and periodic boundary conditions. In each lattice node $\boldsymbol{x}$, we place an Ising spin ($S_{\boldsymbol{x}} = \pm 1$). Lattice nearest-neighbors spins interact through the Hamiltonian $H = -\sum_{\langle \boldsymbol{x},\boldsymbol{y}\rangle} J_{\boldsymbol{xy}} S_{\boldsymbol{x}} S_{\boldsymbol{y}}$. The couplings $J_{\boldsymbol{xy}}$ are independent and identically distributed random variables ($J_{\boldsymbol{xy}} = \pm 1$ with 1/2 probability), fixed when the simulation starts (quenched disorder). This model exhibits a spin-glass transition at temperature $T_c = 1.1019(29)$[58]. We refer to each realization of the couplings as a sample. Statistically independent simulations of a given sample are named replicas. We have considerably extended the simulation of Baity et al.[51], by simulating $N_{\mathrm{Rep}} = 512$ replicas (rather than 256) of the same $N_S = 16$ samples considered in[51], in the temperature range $0.625 \leq T \leq 1.1$.

We simulate the non-equilibrium dynamics with a Metropolis algorithm. In this way, one picosecond of physical time roughly corresponds to a full-lattice Metropolis sweep. At the initial time $t_w = 0$ the spin configuration is fully random (i.e., we quench from infinite temperature). The subsequent growth of spin-glass domains is characterized by the spin-glass coherence length $\xi(t_w)$. Specifically, we use the $\xi_{1,2}$ integral estimators, see refs. [48,51,59,60] for details [the main steps in the computation of $\xi_{1,2}$ are also sketched in Eqs. (8–10)), where one should set $T_1 = T_2 = T$].

Finally, let us briefly comment on our choices for N_{Rep} and N_S. A detailed analysis[51,61] shows that, for a given total numerical effort $N_S \times N_{\mathrm{Rep}}$, errors in ξ are minimized if $N_{\mathrm{Rep}} \gg N_S$. Furthermore, Supplementary Note 1 shows that having $N_{\mathrm{Rep}} \gg 1$ is crucial as well for the main quantities considered in this work (see definitions below). Therefore, given our finite computational resources, we have chosen to limit ourselves to $N_S = 16$. This small number of samples is partly compensated by the fact that we are working close to the experimental regime $L \gg \xi$ [we remark that $N_S = 1$ in typical experiments: indeed, statics-dynamics equivalence suggests that the number of statistically independent events is proportional to $N_S(L/\xi)^3$].

The local chaotic parameter. We shall compare the spin textures from temperature T_1 and waiting time t_{w1} with those from temperature T_2 and waiting time t_{w2} (we consider $T_1 \leq T_2 \leq T_c$). A fair comparison requires that the two configurations be ordered at the same lengthscale, which we ensure by imposing the condition

$$\xi(t_{w1}, T_1) = \xi(t_{w2}, T_2) = \xi \ . \tag{1}$$

A first investigation of TC is shown in Fig. 1. The overlap, computed over the whole sample, of two systems satisfying

condition Eq. (1) is used to search for a coarse-grained chaotic effect. The resulting signal is measurable but weak. Instead, as explained in the introduction, spin configurations should be compared locally. Specifically, we consider spherical regions. We start by choosing $N_{\rm sph} = 8000$ centers for the spheres on each sample. The spheres' centers are chosen randomly, with uniform probability, on the dual lattice which, in a cubic lattice with periodic boundary conditions, is another cubic lattice of the same size, also periodic boundary condition. The nodes of the dual lattice are the centers of the elementary cells of the original lattice. The radii of the spheres are varied, but their centers are held fixed. Let $B_{s,r}$ be the s-th ball of radius r. Our basic observable is the overlap between replica σ (at temperature T_1), and replica $\tau \neq \sigma$ (at temperature T_2):

$$q^{s,r;\sigma,\tau}_{T_1,T_2}(\xi) = \frac{1}{N_r}\sum_{\boldsymbol{x}\in B_{s,r}} s^{\sigma,T_1}_{\boldsymbol{x}}(t_{\rm w1}) s^{\tau,T_2}_{\boldsymbol{x}}(t_{\rm w2}), \qquad (2)$$

where N_r is the number of spins in the ball, and $t_{\rm w1}$ and $t_{\rm w2}$ are chosen according to Eq. (1). Averages over thermal histories, indicated by $\langle \ldots \rangle_T$, are computed by averaging over σ and τ.

Next, we generalize the so-called chaotic parameter[6,16,17,20] as

$$X^{s,r}_{T_1,T_2}(\xi) = \frac{\langle [q^{s,r;\sigma,\tau}_{T_1,T_2}(\xi)]^2 \rangle_T}{\sqrt{\langle [q^{s,r;\sigma,\tau}_{T_1,T_1}(\xi)]^2 \rangle_T \, \langle [q^{s,r;\sigma,\tau}_{T_2,T_2}(\xi)]^2 \rangle_T}}, \qquad (3)$$

The extremal values of the chaotic parameter have a simple interpretation: $X^{s,r}_{T_1,T_2} = 1$ corresponds with a situation in which spin configurations in the ball $B_{s,r}$, at temperatures T_1 and T_2, are completely indistinguishable (absence of chaos) while $X^{s,r}_{T_1,T_2} = 0$ corresponds to completely different configurations (strong TC). A representative example our results is shown in Fig. 2.

Our main focus will be on the distribution function $F(X, T_1, T_2, \xi, r) =$ Probability $[X^{s,r}_{T_1,T_2}(\xi) < X]$ and on its inverse $X(F, T_1, T_2, \xi, r)$.

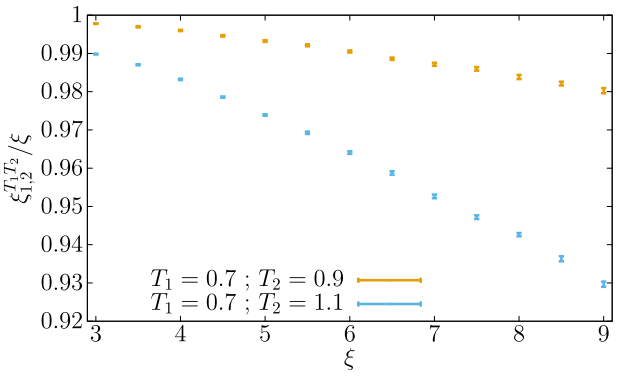

Fig. 1 Non-equilibrium temperature chaos is weak when averaging over the whole system. We compare typical spin configurations at temperature T_1 and time $t_{\rm w1}$ with configurations at T_2 and time $t_{\rm w2}$. The comparison is carried through a global estimator of the coherence length of their overlap $\xi^{T_1T_2}_{1,2}$ which represents the maximum lengthscale at which configurations at temperatures T_1 and T_2 still look similar, see Methods section for further details. The two times $t_{\rm w1}$ and $t_{\rm w2}$ are chosen in such a way that the configurations at both temperatures have glassy-domains of the same size, namely $\xi_{1,2}(t_{\rm w1}, T_1) = \xi_{1,2}(t_{\rm w2}, T_2) = \xi$. The figure shows the ratio $\xi^{T_1T_2}_{1,2}/\xi$ as a function of ξ for two pairs of temperatures (T_1, T_2), recall that $T_c \approx 1.1$[58]. Under the hypothesis of fully developed Temperature Chaos, we would expect $\xi^{T_1T_2}_{1,2}$ to be negligible compared to ξ. Instead, our data shows only a small decrease of $\xi^{T_1T_2}_{1,2}/\xi$ with growing ξ (the larger the difference $T_2 - T_1$ the more pronounced the decrease). Error bars represent one standard deviation.

The rare-event analysis. Representative examples of distribution functions $F(X, T_1, T_2, \xi, r)$ are shown in Fig. 3. We see that, in close analogy with equilibrium systems[16,17,19], while most spheres exhibit a very weak TC ($X > 0.9$, say), there is a fraction of spheres

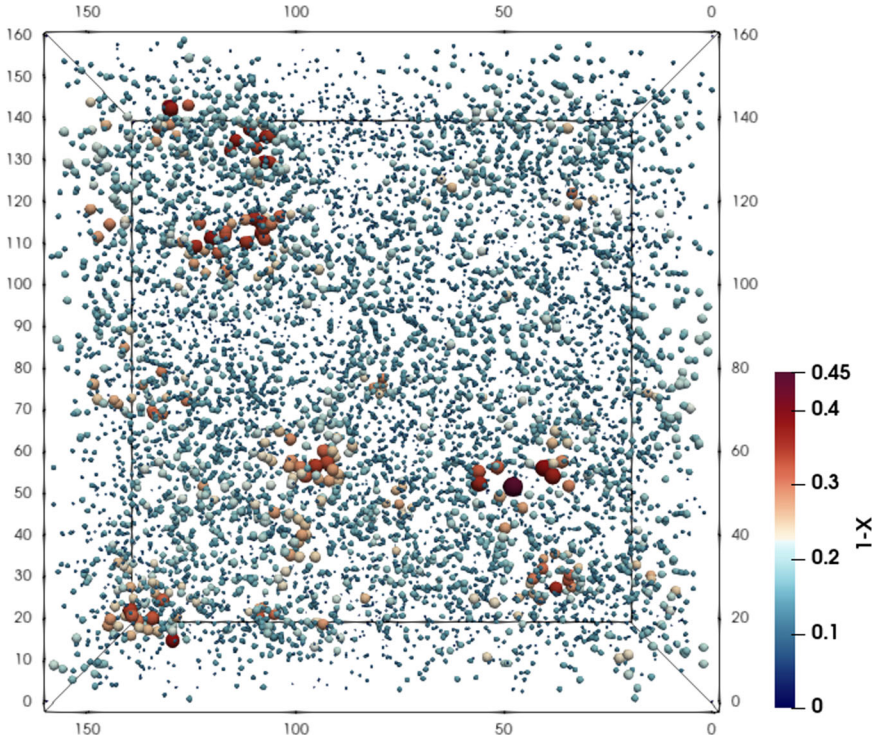

Fig. 2 Dynamic temperature chaos is spatially heterogeneous. The 8000 randomly chosen spheres in a sample of size $L = 160$ are depicted with a color code depending on $1 - X$ [X is the chaotic parameter, Eq. (3), as computed for spheres of radius $r = 12$, $\xi = 12$ and temperatures $T_1 = 0.7$ and $T_2 = 1.0$]. For visualization purposes, spheres are represented with a radius $12(1 - X)$, so that only fully chaotic spheres (i.e., $X = 0$) have their real size.

displaying smaller X (stronger chaos). Note that the probability F of finding spheres with X smaller than any prefixed value increases when ξ grows.

In order to make the above finding quantitative, we consider the (inverse) distribution function $X(F, T_1, T_2, \xi, r)$. We start by fixing (T_1, T_2), ξ and some small probability F, which leaves us with a function of only r. In order to obtain smoother interpolations for small radius, however, we have used $N_r^{1/3}$ instead of r as our independent variable, a technical detailed discussion can be found in Supplementary Note 3.

Figure 4 shows plots of $1 - X$ under these conditions, which exhibit well-defined peaks (see further information about the fitting function to the peaks in the Supplementary Note 2). Now, to a first approximation we can characterize any peak by its position, height and width. Fortunately, these three parameters turn out to describe the scaling with ξ of the full $1 - X$ curve, see Supplementary Note 4.

The physical interpretation of the peak's parameters is clear. The peak's height represents the strength of dynamic TC (the taller the peak, the larger the chaos). The peak's position indicates the optimal lengthscale for the study of TC, given the probability F, ξ and the temperatures T_1, T_2. The peak's width indicates how critical it is to spot this optimal lengthscale (the wider the peak, the less critical the choice). Perhaps unsurprisingly, the peak's position is found to scale linearly with ξ, while the peak's width scales as ξ^β, with β slightly larger than one, see Supplementary Note 5 for further details. We shall focus here on the temperature and ξ dependence of the peak's height (i.e., the strength of chaos), which has a richer behavior.

The ξ dependence of the peak's height (for a given probability F and temperatures T_1 and T_2) turns out to be reasonably well described by the following ansatz:

$$f_{\max}(\xi) = \frac{\varepsilon(\xi)}{1+\varepsilon(\xi)} \ , \ \text{with}\ \varepsilon(\xi) = (\xi/\xi^*)^\alpha \ . \tag{4}$$

This formula describes a crossover phenomenon, ruled by a characteristic length ξ^*. For $\xi \ll \xi^*$ the peak's height grows with ξ as a power law, while for $\xi \gg \xi^*$ the strong-chaos limit [i.e., $(1 - X) \to 1$] is approached. However, some consistency requirements should be met before taking the crossover length ξ^* seriously. Not only should the fit to Eq. (4) be of acceptable statistical quality (the fit parameters are the characteristic lengthscale ξ^* and the exponent α). One would also wish exponent α to be independent of the temperatures T_1 and T_2 and of the chosen probability F.

We find fair fits to Eq. (4), see Table 1. In all cases, exponent α turns out to be compatible with 2.1 at the two-σ level [except for the $(F = 0.01, T_1 = 0.625, T_2 = 0.8)$ fit]. Under these conditions, we can interpret ξ^* as a characteristic length indicating the crossover from weak to strong TC, at the probability level indicated by F. Furthermore, the relatively large value of exponent α indicates that this crossover is sharp.

The trends for the crossover length ξ^* in Table 1 are very clear: ξ^* grows upon increasing F or upon decreasing $T_2 - T_1$. Identifying ξ^* as the non-equilibrium partner of the equilibrium chaotic length $\ell_c(T_1, T_2)$[3,56] will allow us to be more quantitative (indeed, the two lengthscales indicate the crossover between weak

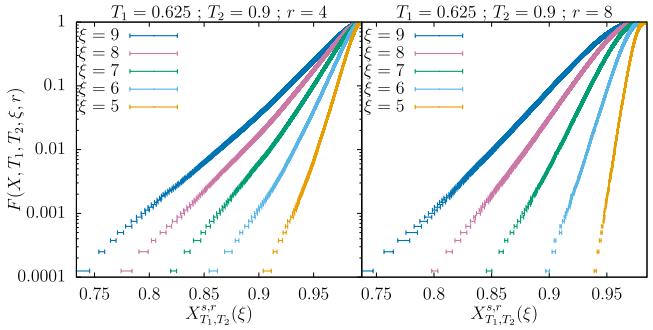

Fig. 3 Temperature chaos increases with the coherence length. The figure shows the distribution function $F(X, T_1, T_2, \xi, r)$ for temperatures $T_1 = 0.625$ and $T_2 = 0.9$, for spheres of radius $r = 4$ and $r = 8$, as computed for various values of ξ. The distributions have been extrapolated to infinite number of replicas $N_{\text{Rep}} = \infty$, see Supplementary Note 1 for further details. Error bars, that represent one standard deviation, are horizontal, because we have actually extrapolated the chaotic parameter, which is its inverse function $X(F, T_1, T_2, \xi, r)$. Most of the spheres have a chaotic parameter very close to $X = 1$ (absence of chaos). However, if we fix our attention, for instance, on percentile 1 (i.e., $F = 0.01$) we see that the corresponding value of X decreases monotonically (and significantly) as ξ grows, signaling a developing chaotic effect. This trend is clear both for spheres of radius $r = 4$ and $r = 8$.

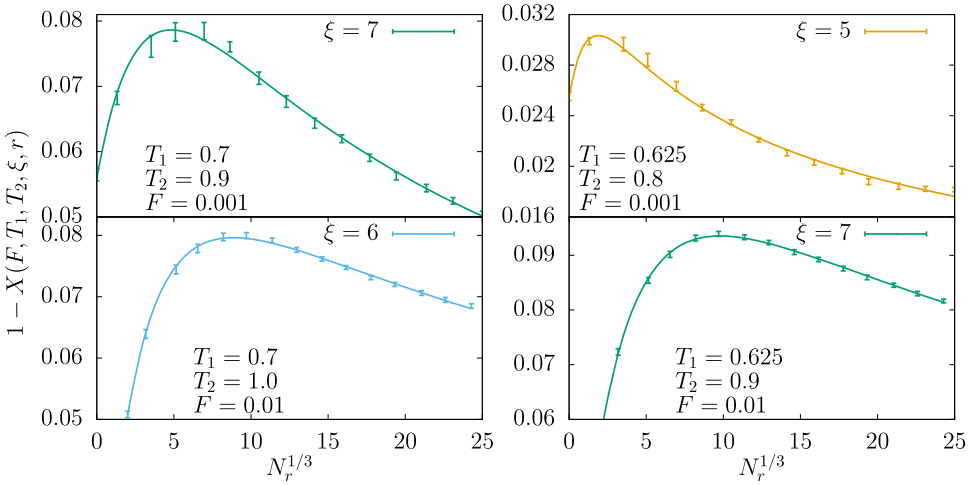

Fig. 4 Emergence of an optimal scale to observe temperature chaos. The difference $1 - X(F, T_1, T_2, \xi, r)$ [recall that $X(F, T_1, T_2, \xi, r)$ is the inverse of the distribution function] as a function of the cubic root $N_r^{1/3}$ of the number of spins in the spheres, as computed for different values of the probability level F, the temperatures T_1 and T_2, and the coherence length ξ. In this representation, the optimal size of the spheres for the observation of chaos (for given parameters F, T_1, T_2 and ξ) appears as the maximum of the curves. Continuous lines are fits to a smooth interpolating function, further details can be found in Supplementary Note 2. Error bars represent one standard deviation.

Table 1 Parameters describing the crossover between weak and strong temperature chaos regimes.

F	T_1	T_2	ξ_{min}	ξ^*	α	χ^2/d.o.f
0.001	0.625	0.7	4.75	55(4)	2.10(7)	14.10/19
0.001	0.625	0.8	5.25	24.1(8)	2.18(6)	22.67/17
0.001	0.625	0.9	4.75	16.8(3)	2.09(4)	28.88/19
0.001	0.625	1.0	4.75	13.24(15)	2.04(3)	8.77/19
0.001	0.7	0.8	4.75	43.5(15)	2.12(5)	41.05/28
0.001	0.7	0.9	4.75	22.9(5)	2.09(4)	33.32/28
0.001	0.7	1.0	4.75	16.3(2)	2.04(4)	22.32/28
0.01	0.625	0.8	5.75	29.3(5)	2.21(3)	13.32/15
0.01	0.625	0.9	5.75	20.5(3)	2.12(2)	16.05/15
0.01	0.625	1.0	4.75	15.87(16)	2.08(2)	23.93/19
0.01	0.7	0.8	4.75	51.4(12)	2.17(3)	8.06/28
0.01	0.7	0.9	5.25	27.9(4)	2.11(2)	31.56/26
0.01	0.7	1.0	4.75	19.9(2)	2.05(2)	31.78/28

Parameters obtained in the fits to Eq. (4) of our data for the peak's height, see Fig. 4, with $\xi_{min} \le \xi \le \xi_{max}$. We also report the fits' figure of merit χ^2/d.o.f. We chose ξ_{min} by requiring a P value greater than 0.05 in the fits ($\xi_{max} = 9.5$ for $T_1 = 0.625$ and $\xi_{max} = 12.5$ for $T_1 = 0.7$). T_1 and T_2 represent the temperatures involved in the computation of the chaotic parameter. Unfortunately, the flatness of the peak for ($T_1 = 0.625$, $T_2 = 0.7$, $F = 0.01$) did not allow us to compute the peak's parameters.

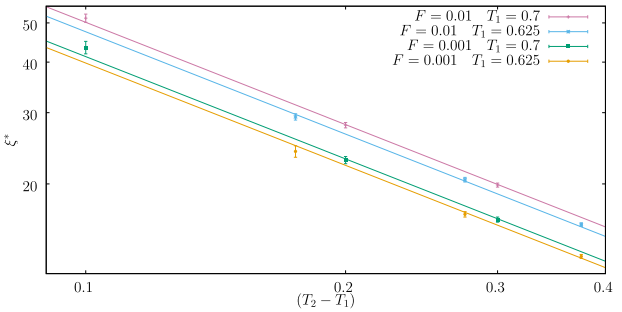

Fig. 5 Universal scaling of dynamic chaos. The characteristic length ξ^* is plotted against the temperature difference $T_2 - T_1$ in a log-log scale. Each curve is uniquely identified by the probability level F and the smallest temperature of each pair T_1. Fits to Eq. (6), enforcing a common exponent, are shown with continuous lines and result in a chaotic exponent $\zeta_{NE} =$ 1.19(2). Error bars represent one standard deviation.

chaos and strong chaos). Now, the equilibrium $\ell_c(T_1, T_2)$ has been found to scale for the 3D Ising spin glass as

$$\ell_c(T_1, T_2) \propto (T_2 - T_1)^{-1/\zeta} \quad , \tag{5}$$

with $\zeta \approx 1.07$[14] or $\zeta \approx 1.07(5)$[16]. These considerations suggest the following ansatz for the non-equilibrium crossover length

$$\xi^*(T_1, T_2, F) = B(F, T_1)\ (T_2 - T_1)^{-1/\zeta_{NE}} \quad , \tag{6}$$

where $B(F, T_1)$ is an amplitude. We have tested Eq. (6) by computing a joint fit for four (T_1, F) pairs as functions of $T_2 - T_1$, allowing each curve to have its own amplitude but enforcing a common ζ_{NE} (see Fig. 5). The resulting χ^2/d.o.f. = 7.55/7 validates our ansatz, with an exponent $\zeta_{NE} = 1.19(2)$ fairly close to the equilibrium result $\zeta = 1.07(5)$[16]. This agreement strongly supports our physical interpretation of the crossover length. We, furthermore, find that B is only weakly dependent on T_1. Nevertheless, the reader should be warned that it has been suggested[16] that the equilibrium exponent ζ may be different in the weak- and strong-chaos regimes.

Conclusions

We have shown that the concept of temperature chaos can be meaningfully extended to the non-equilibrium dynamics of a large spin glass. This is, precisely, the framework for rejuvenation and memory experiments[28–31], as well as other more chaos-oriented experimental work[57]. Therefore, our precise characterization of dynamical temperature chaos paves the way for the interpretation of these and forthcoming experiments. Our simulation of spin-glass dynamics doubles the numerical effort in[51] and has been carried out on the Janus-II special-purpose supercomputer.

The key quantity governing dynamic temperature chaos is the time-dependent spin-glass coherence length $\xi(t_w)$. The very strong spatial heterogeneity of this phenomenon is quantified through a distribution function F. This probability can be thought of as the fraction of the sample that shows a chaotic response to a given degree. When comparing temperatures T_1 and T_2, the degree of chaoticity is governed by a lengthscale $\xi^*(F, T_1, T_2)$. While chaos is very weak if $\xi(t_w) \ll \xi^*(F, T_1, T_2)$, it quickly becomes strong as $\xi(t_w)$ approaches $\xi^*(F, T_1, T_2)$. We find that, when T_1 approaches T_2, $\xi^*(F, T_1, T_2)$ appears to diverge with the same critical exponent that it is found for the equilibrium chaotic length[16].

Although we have considered in this work fairly small values of the chaotic system fraction F, a simple extrapolation, linear in log F, predicts $\xi^* \approx 60$ for $F = 0.1$ at $T_1 = 0.7$ and $T_2 = 0.8$ (our closest pair of temperatures in Table 1). A spin-glass coherence length well above $60a_0$ is experimentally reachable nowadays[52,57,62,63] (a_0 is the typical spacing between spins), which makes our dynamic temperature chaos significant. Indeed, while completing this manuscript, a closely related experimental study[57] reported a value for exponent ζ_{NE} in fairly good agreement with our result of $\zeta_{NE} =$ 1.19(2) in Fig. 5.

Let us conclude by commenting on possible venues for future research. Clearly, it will be important to understand in detail how dynamic temperature chaos manifests itself in non-equilibrium experiments. Simple protocols (in which temperature sharply drops from T_2 to T_1, see, e.g., Zhai et. al.[57]) seems more accessible to a first analysis than memory and rejuvenation experiments[28–31]. An important problem is that the correlation functions that are studied theoretically are not easily probed experimentally. Instead, experimentalists privilege the magnetization density (which is a spatial average over the whole sample). Therefore an important theoretical goal is to predict the behavior of the non-equilibrium time-dependent magnetization upon a temperature drop. One may speculate that the Generalized Fluctuation-Dissipation Relations[64] might be the route connecting the correlation functions with the response to an externally applied magnetic field. Interestingly enough, these relations (that apply at fixed temperature) can be defined locally as well[65]. The resulting spatial distribution function allows the reconstruction of the global response to the magnetic field. Extending this analysis to a temperature drop may turn out to be fruitful in the future.

Methods

All the observables involved in the computation of temperature chaos depend on a pair of replicas (σ, τ). The basic quantity is the overlap field

$$q^{\sigma,\tau}(\boldsymbol{x}, t_w) = s^{\sigma}_{\boldsymbol{x}}(t_w) s^{\tau}_{\boldsymbol{x}}(t_w), \tag{7}$$

Usually, this pair of replicas are at the same temperature T. All the definitions are, however, straightforwardly extended to two temperatures. For instance, the four-point two-temperature spatial correlation function is

$$C_4^{T_1 T_2}(T_1, T_2, t_{w1}, t_{w2}, \boldsymbol{r}) = \left[\langle q^{\sigma(T_1),\tau(T_2)}(\boldsymbol{x}, t_{w1}, t_{w2}) q^{\sigma(T_1),\tau(T_2)}(\boldsymbol{x} + \boldsymbol{r}, t_{w1}, t_{w2}) \rangle_T \right]_J, \tag{8}$$

where $[\ldots]_J$ denotes the average over the samples. Building on this function we can

define our integral estimator for the coherence length[60]:

$$I_k^{T_1T_2}(t_{w1}, t_{w2}) = \int_0^\infty r^k \; C_4^{T_1T_2}(r, t_{w1}, t_{w2}) \; \mathrm{d}r, \tag{9}$$

and

$$\xi_{k,k+1}^{T_1T_2}(t_{w1}, t_{w2}) = \frac{I_{k+1}^{T_1T_2}(t_{w1}, t_{w2})}{I_k^{T_1T_2}(t_{w1}, t_{w2})}. \tag{10}$$

As explained in the main text, times t_{w1} and t_{w2} are fixed through the condition expressed in Eq. (1), which ensures that we are comparing spin configurations that are ordered on the same length scale.

Since our t_w are on a discrete grid, we solve Eq. (1) for the global overlaps through a (bi)linear interpolation.

Data availability

The data contained in the figures of this paper, accompanied by the gnuplot script files that generate these figures, are publicly available at https://github.com/JanusCollaboration/caosdin.

The data that support the findings of this study are available from the corresponding author upon reasonable request.

Code availability

The codes that support the findings of this study are available from the corresponding author upon reasonable request.

Received: 1 December 2020; Accepted: 26 February 2021;
Published online: 13 April 2021

References

1. Young, A. P. *Spin Glasses and Random Fields*. (World Scientific, Singapore, 1998).
2. McKay, S. R., Berker, A. N. & Kirkpatrick, S. Spin-glass behavior in frustrated Ising models with chaotic renormalization-group trajectories. *Phys. Rev. Lett.* **48**, 767 (1982).
3. Bray, A. J. & Moore, M. A. Chaotic nature of the spin-glass phase. *Phys. Rev. Lett.* **58**, 57 (1987).
4. Banavar, J. R. & Bray, A. J. Chaos in spin glasses: a renormalization-group study. *Phys. Rev. B* **35**, 8888 (1987).
5. Kondor, I. On chaos in spin glasses. *J. Phys. A* **22**, L163 (1989).
6. Ney-Nifle, M. & Young, A. P. Chaos in a two-dimensional Ising spin glass. *J. Phys. A* **30**, 5311 (1997).
7. Ney-Nifle, M. Chaos and universality in a four-dimensional spin glass. *Phys. Rev. B* **57**, 492 (1998).
8. Billoire, A. & Marinari, E. Evidence against temperature chaos in mean-field and realistic spin glasses. *J. Phys. A* **33**, L265 (2000).
9. Mulet, R., Pagnani, A. & Parisi, G. Against temperature chaos in naive thouless-anderson-palmer equations. *Phys. Rev. B* **63**, 184438 (2001).
10. Billoire, A. & Marinari, E. Overlap among states at different temperatures in the SK model. *Europhys. Lett.* **60**, 775 (2002).
11. Krzakala, F. & Martin, O. C. Chaotic temperature dependence in a model of spin glasses. *Eur. Phys. J. B* **28**, 199 (2002).
12. Rizzo, T. & Crisanti, A. Chaos in temperature in the Sherrington-Kirkpatrick model. *Phys. Rev. Lett.* **90**, 137201 (2003).
13. Sasaki, M., Hukushima, K., Yoshino, H. & Takayama, H. Temperature chaos and bond chaos in Edwards-Anderson Ising spin glasses: domain-wall free-energy measurements. *Phys. Rev. Lett.* **95**, 267203 (2005).
14. Katzgraber, H. G. & Krzakala, F. Temperature and disorder chaos in three-dimensional Ising spin glasses. *Phys. Rev. Lett.* **98**, 017201 (2007).
15. Parisi, G. & Rizzo, T. Chaos in temperature in diluted mean-field spin-glass. *J. Phys. A* **43**, 235003 (2010).
16. Fernandez, L. A., Martín-Mayor, V., Parisi, G. & Seoane, B. Temperature chaos in 3d Ising spin glasses is driven by rare events. *EPL* **103**, 67003 (2013).
17. Billoire, A. Rare events analysis of temperature chaos in the Sherrington-Kirkpatrick model. *J. Stat. Mech.* **2014**, P04016 (2014).
18. Wang, W., Machta, J. & Katzgraber, H. G. Chaos in spin glasses revealed through thermal boundary conditions. *Phys. Rev. B* **92**, 094410 (2015).
19. Billoire, A. et al. Dynamic variational study of chaos: spin glasses in three dimensions. *J. Stat. Mech. Theory Exp.* **2018**, 033302 (2018).
20. Ritort, F. Static chaos and scaling behavior in the spin-glass phase. *Phys. Rev. B* **50**, 6844 (1994).
21. Billoire, A. & Coluzzi, B. Magnetic field chaos in the Sherrington-Kirkpatrick model. *Phys. Rev. E* **67**, 036108 (2003).
22. Komori, T., Yoshino, H. & Takayama, H. Numerical study on aging dynamics in the 3d Ising spin-glass model. II. quasi-equilibrium regime of spin auto-correlation function. *J. Phys. Soc. Japan* **69**, 1192 (2000).
23. Berthier, L. & Bouchaud, J.-P. Geometrical aspects of aging and rejuvenation in the Ising spin glass: a numerical study. *Phys. Rev. B* **66**, 054404 (2002).
24. Picco, M., Ricci-Tersenghi, F. & Ritort, F. Chaotic, memory, and cooling rate effects in spin glasses: evaluation of the Edwards-Anderson model. *Phys. Rev. B* **63**, 174412 (2001).
25. Takayama, H. & Hukushima, K. Numerical study on aging dynamics in the 3d Ising spin-glass model: III. cumulative memory andchaos' effects in the temperature-shift protocol. *J. Phys. Soc. Japan* **71**, 3003 (2002).
26. Maiorano, A., Marinari, E. & Ricci-Tersenghi, F. Edwards-anderson spin glasses undergo simple cumulative aging. *Phys. Rev. B* **72**, 104411 (2005).
27. Jiménez, S., Martín-Mayor, V. & Pérez-Gaviro, S. Rejuvenation and memory in model spin glasses in three and four dimensions. *Phys. Rev. B* **72**, 054417 (2005).
28. Jonason, K., Vincent, E., Hammann, J., Bouchaud, J. P. & Nordblad, P. Memory and chaos effects in spin glasses. *Phys. Rev. Lett.* **81**, 3243 (1998).
29. Lundgren, L., Svedlindh, P. & Beckman, O. Anomalous time dependence of the susceptibility in a Cu(Mn) spin glass. *J. Magn. Magn. Mater.* **31-34**, 1349 (1983).
30. Jonsson, T., Jonason, K., Jönsson, P. E. & Nordblad, P. Nonequilibrium dynamics in a three-dimensional spin glass. *Phys. Rev. B* **59**, 8770 (1999).
31. Hammann, J. et al. Comparative review of aging properties in spin glasses and other disordered materials. *J. Phys. Soc. Jpn.* **206** (2000).
32. Ozon, F. et al. Partial rejuvenation of a colloidal glass. *Phys. Rev. E* **68**, 032401 (2003).
33. Bellon, L., Ciliberto, S. & Laroche, C. Memory in the aging of a polymer glass. *Europhys. Lett.* **51**, 551 (2000).
34. Yardimci, H. & Leheny, R. L. Memory in an aging molecular glass. *Europhys. Lett.* **62**, 203 (2003).
35. Bouchaud, J.-P., Doussineau, P., de Lacerda-Arôso, T. & Levelut, A. Frequency dependence of aging, rejuvenation and memory in a disordered ferroelectric. *Eur. Phys. J. B* **21**, 335 (2001).
36. Mueller, V. & Shchur, Y. Aging, rejuvenation and memory due to domain-wall contributions in RbH_2 PO_4 single crystals. *Europhys. Lett.* **65**, 137 (2004).
37. Subag, E. The geometry of the Gibbs measure of pure spherical spin glasses. *Inventiones Math.* **210**, 135 (2017).
38. Kurchan, J., Parisi, G. & Virasoro, M. A. Barriers and metastable states as saddle points in the replica approach. *J. Phys. I France* **3**, 1819 (1993).
39. Barrat, A., Franz, S. & Parisi, G. Temperature evolution and bifurcations of metastable states in mean-field spin glasses, with connections with structural glasses. *J. Phys. A* **30**, 5593 (1997).
40. Chen, W. K. Chaos in the mixed even-spin models. *Commun. Math. Phys.* **328**, 867 (2014).
41. Panchenko, D. Chaos in temperature in generic 2p-spin models. *Commun. Math. Phys.* **346**, 703 (2016).
42. Chen, W. K. & Panchenko, D. Temperature chaos in some spherical mixed p-spin models. *J. Stat. Phys.* **166**, 1151 (2017).
43. Arous, G. B., Subag, E. & Zeitouni, O. Geometry and temperature chaos in mixed spherical spin glasses at low temperature: The perturbative regime. *Commun. Pure Appl. Math.* **73**, 1732 (2020).
44. Edwards, S. F. & Anderson, P. W. Theory of spin glasses. *J. Phys F Metal Phys.* **5**, 965 (1975).
45. Edwards, S. F. & Anderson, P. W. Theory of spin glasses. ii. *J. Phys. F* **6**, 1927 (1976).
46. Baity-Jesi, M. et al. (Janus Collaboration). Janus II: a new generation application-driven computer for spin-system simulations. *Comp. Phys. Comm.* **185**, 550 (2014).
47. Barrat, A. & Berthier, L. Real-space application of the mean-field description of spin-glass dynamics. *Phys. Rev. Lett.* **87**, 087204 (2001).
48. Belletti, F. et al. (Janus Collaboration). Nonequilibrium spin-glass dynamics from picoseconds to one tenth of a second. *Phys. Rev. Lett.* **101**, 157201 (2008).
49. AlvarezBaños, R. et al. (Janus Collaboration). Static versus dynamic heterogeneities in the $D = 3$ Edwards-Anderson-Ising spin glass. *Phys. Rev. Lett.* **105**, 177202 (2010).
50. Baity-Jesi, M. et al. A statics-dynamics equivalence through the fluctuation-dissipation ratio provides a window into the spin-glass phase from nonequilibrium measurements. *Proc. Natl Acad. Sci. USA* **114**, 1838 (2017).
51. Baity-Jesi, M. et al. (Janus Collaboration). Aging rate of spin glasses from simulations matches experiments. *Phys. Rev. Lett.* **120**, 267203 (2018).
52. Zhai, Q., Martin-Mayor, V., Schlagel, D. L., Kenning, G. G. & Orbach, R. L. Slowing down of spin glass correlation length growth: Simulations meet experiments. *Phys. Rev. B* **100**, 094202 (2019).
53. Billoire, A. et al. Finite-size scaling analysis of the distributions of pseudo-critical temperatures in spin glasses. *J. Stat. Mech.* **2011**, P10019 (2011).
54. Martín-Mayor, V. & Hen, I. Unraveling quantum annealers using classical hardness. *Sci. Rep.* **5**, 15324 (2015).
55. Fernández, L. A., Marinari, E., Martín-Mayor, V., Parisi, G. & Yllanes, D. Temperature chaos is a non-local effect. *J. Stat. Mech. Theory Exp.* **2016**, 123301 (2016).

56. Fisher, D. S. & Huse, D. A. Ordered phase of short-range Ising spin-glasses. *Phys. Rev. Lett.* **56**, 1601 (1986).
57. Zhai, R. L., Qiang ad Orbach & Schlagel, D. Spin glass correlation length: a caliper for temperature chaos. Preprint at http://arxiv.org/abs/arXiv:2010.01214 (2020).
58. Baity-Jesi, M. et al. (Janus Collaboration). Critical parameters of the three-dimensional Ising spin glass. *Phys. Rev. B* **88**, 224416 (2013).
59. Fernández, L. A., Marinari, E., Martín-Mayor, V., Parisi, G. & Ruiz-Lorenzo, J. An experiment-oriented analysis of 2d spin-glass dynamics: a twelve time-decades scaling study. *J. Phys. A* **52**, 224002 (2019).
60. Belletti, F. et al. (Janus Collaboration). An in-depth look at the microscopic dynamics of Ising spin glasses at fixed temperature. *J. Stat. Phys.* **135**, 1121 (2009).
61. Fernandez, L. A., Marinari, E., Martin-Mayor, V., Paga, I. & Ruiz-Lorenzo, J. J. Dimensional crossover in the aging dynamics of spin glasses in a film geometry. *Phys. Rev. B* **100**, 184412 (2019).
62. Zhai, Q. et al. Scaling law describes the spin-glass response in theory, experiments, and simulations. *Phys. Rev. Lett.* **125**, 237202 (2020).
63. Paga, I. et al. Spin-glass dynamics in the presence of a magnetic field: exploration of microscopic properties. *J. Stat. Mech. Theory Exp.* **2021**, 033301 (2021).
64. Cugliandolo, L. F. & Kurchan, J. Analytical solution of the off-equilibrium dynamics of a long-range spin-glass model. *Phys. Rev. Lett.* **71**, 173 (1993).
65. Castillo, H. E., Chamon, C., Cugliandolo, L. F. & Kennett, M. P. Heterogeneous aging in spin glasses. *Phys. Rev. Lett.* **88**, 237201 (2002).

Acknowledgements

We are grateful for discussions with R. Orbach and Q. Zhai. This work was partially supported by Ministerio de Economía, Industria y Competitividad (MINECO, Spain), Agencia Estatal de Investigación (AEI, Spain), and Fondo Europeo de Desarrollo Regional (FEDER, EU) through Grants No. FIS2016-76359-P, No. PID2019-103939RB-I00, No. PGC2018-094684-B-C21 and PGC2018-094684-B-C22, by the Junta de Extremadura (Spain) and Fondo Europeo de Desarrollo Regional (FEDER, EU) through Grant No. GRU18079 and IB15013 and by the DGA-FSE (Diputación General de Aragón – Fondo Social Europeo). This project has also received funding from the European Research Council (ERC) under the European Union's Horizon 2020 research and innovation program (Grant No. 694925-LotglasSy). DY was supported by the Chan Zuckerberg Biohub and IGAP was supported by the Ministerio de Ciencia, Innovación y Universidades (MCIU, Spain) through FPU grant no. FPU18/02665. BS was supported by the Comunidad de Madrid and the Complutense University of Madrid (Spain) through the Atracción de Talento program (Ref. 2019-T1/TIC-12776).

Author contributions

J.M.G.-N. and D.N. contributed to Janus/Janus II simulation software. D.I., A.T. and R.T. contributed to Janus II design. M.B.-J., E.C., A.C., L.A.F, J.M.G.-N., I.G.-A.P., A.G.-G., D.I., A.M., A.M.-S., I.P., S.P.-G., S.F.S., A.T. and R.T. contributed to Janus II hardware and software development. L.A.F., V.M.-M. and J.M.-G. designed the research. J.M.-G. analyzed the data. M.B.-J., L.A.F., E.M., V.M.-M., J.M.-G., I.P., G.P., B.S., J.J.R.-L., F.R.-T. and D.Y. discussed the results. V.M.-M., J.M.-G., B.S. and D.Y. wrote the paper.

Competing interests

The authors declare no competing interests.

Additional information

Supplementary information The online version contains supplementary material available at https://doi.org/10.1038/s42005-021-00565-9.

Correspondence and requests for materials should be addressed to J.M-G.

Reprints and permission information is available at http://www.nature.com/reprints

Publisher's note Springer Nature remains neutral with regard to jurisdictional claims in published maps and institutional affiliations.

Supplemental Material: Temperature chaos is present in off-equilibrium spin-glass dynamics.

Marco Baity-Jesi,[1] Enrico Calore,[2] Andrés Cruz,[3,4] Luis Antonio Fernandez,[5,4] José Miguel Gil-Narvion,[4] Isidoro Gonzalez-Adalid Pemartin,[5] Antonio Gordillo-Guerrero,[6,7,4] David Iñiguez,[4,8,3] Andrea Maiorano,[9,10,4] Enzo Marinari,[11,10] Víctor Martin-Mayor,[5,4] Javier Moreno-Gordo,[4,3,*] Antonio Muñoz-Sudupe,[5,4] Denis Navarro,[12] Ilaria Paga,[13,5] Giorgio Parisi,[11,10] Sergio Perez-Gaviro,[14,4,3] Federico Ricci-Tersenghi,[11,10] Juan Jesús Ruiz-Lorenzo,[15,7,4] Sebastiano Fabio Schifano,[16] Beatriz Seoane,[5,4] Alfonso Tarancon,[3,4] Raffaele Tripiccione,[2] and David Yllanes[17,4]

(Janus Collaboration)

[1] *Eawag, Überlandstrasse 133, CH-8600 Dübendorf, Switzerland*
[2] *Dipartimento di Fisica e Scienze della Terra, Università di Ferrara e INFN, Sezione di Ferrara, I-44122 Ferrara, Italy*
[3] *Departamento de Física Teórica, Universidad de Zaragoza, 50009 Zaragoza, Spain*
[4] *Instituto de Biocomputación y Física de Sistemas Complejos (BIFI), 50018 Zaragoza, Spain*
[5] *Departamento de Física Teórica, Universidad Complutense, 28040 Madrid, Spain*
[6] *Departamento de Ingeniería Eléctrica, Electrónica y Automática, U. de Extremadura, 10003, Cáceres, Spain*
[7] *Instituto de Computación Científica Avanzada (ICCAEx), Universidad de Extremadura, 06006 Badajoz, Spain*
[8] *Fundación ARAID, Diputación General de Aragón, 50018 Zaragoza, Spain*
[9] *Dipartimento di Biotecnologie, Chimica e Farmacia, Università degli studi di Siena, 53100, Siena, Italy*
[10] *INFN, Sezione di Roma 1, I-00185 Rome, Italy*
[11] *Dipartimento di Fisica, Sapienza Università di Roma, and CNR-Nanotec, I-00185 Rome, Italy*
[12] *Departamento de Ingeniería, Electrónica y Comunicaciones and I3A, U. de Zaragoza, 50018 Zaragoza, Spain*
[13] *Dipartimento di Fisica, Sapienza Università di Roma, INFN, Sezione di Roma 1, I-00185 Rome,Italy*
[14] *Centro Universitario de la Defensa, 50090 Zaragoza, Spain*
[15] *Departamento de Física, Universidad de Extremadura, 06006 Badajoz, Spain*
[16] *Dipartimento di Scienze Chimiche e Farmaceutiche, Università di Ferrara e INFN Sezione di Ferrara, I-44122 Ferrara, Italy*
[17] *Chan Zuckerberg Biohub, San Francisco, CA, 94158*

(Dated: February 25, 2021)

SUPPLEMENTARY NOTE 1: EXTRAPOLATION TO INFINITE REPLICAS

The thermal expectation values necessary to compute the chaotic parameter are defined in the limit of infinite replicas, so an extrapolation is necessary to avoid bias. Fortunately, with all other parameters fixed, the evolution of $X(F, T_1, T_2, \xi, r)$ with $N_{\rm Rep}$ is smooth (see Fig. S1 and Fig. S2). We have mainly used a linear ansatz for the extrapolation,

$$X_{N_{\rm Rep}} = X_\infty + \frac{A}{N_{\rm Rep}} \quad , \tag{S1}$$

where $X_{N_{\rm Rep}}$ is shorthand for $X(F, T_1, T_2, \xi, r; N_{\rm Rep})$, $X_\infty = X(F, T_1, T_2, \xi, r; N_{\rm Rep} \to \infty)$ and A is a constant. As a check for the linear ansatz in Eq. (S1), we have considered two alternative functional forms:

$$X_{N_{\rm Rep}} = X_\infty + \frac{B}{N_{\rm Rep}} + \frac{C}{N_{\rm Rep}^2} \quad , \tag{S2}$$

$$X_{N_{\rm Rep}} = X_\infty + \frac{D}{N_{\rm Rep}^\gamma} \quad , \tag{S3}$$

where B, C and D are amplitudes and γ is a free exponent. We perform independent fits to Eq. (S1), Eq. (S2) and Eq. (S3) for every value of the parameters (F, T_1, T_2, ξ, r). We reject fits with a diagonal $\chi^2/\text{d.o.f} \geq 1.1$. Errors in X_∞ are computed by performing separate fits for each jackknife block (the fitting procedure consists in minimizing the diagonal χ^2, see [1]).

As a first check, we compare the linear and quadratic extrapolations (see Fig.S1 for an illustrative example). The figure shows that even for our largest $N_{\rm Rep}$, namely $N_{\rm Rep} = 256$ and $N_{\rm Rep} = 512$, we are still far from the $N_{\rm Rep} \to \infty$ limit. Fortunately, the linear and the quadratic extrapolations yield compatible results in our region of interest, i.e., the tail of the distribution function. We remark that the consistency condition $\chi^2/\text{d.o.f} < 1.1$ is met in a larger range for the quadratic extrapolation ($F < 0.9$) than for the linear extrapolation ($F < 0.7$). However, because both coincide in the low-F range we are interested in, we have kept the simpler linear extrapolation.

Our second check in Eq. (S3) seeks the natural exponent γ for the extrapolation as a fitting parameter. We have found that the consistency condition $\chi^2/\text{d.o.f} < 1.1$ is met for $F < 0.85$. Fortunately, γ turns out to be very close to the value $\gamma = 1$, with the exception of an insta-

* ORCID:0000-0002-0420-8605 jmorenogordo@gmail.com

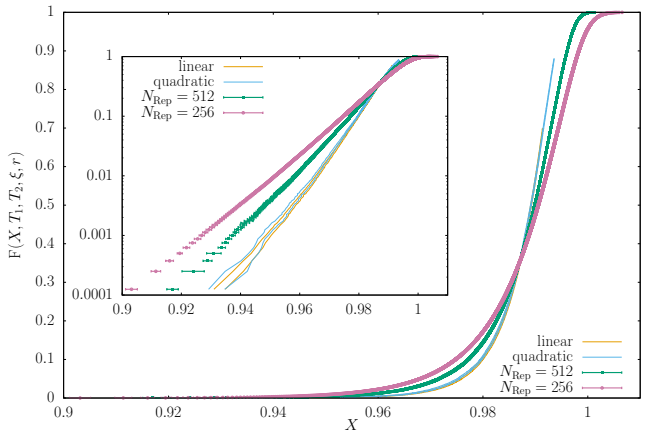

FIG. S1. Linear and quadratic extrapolations, Eq. (S1) and Eq. (S2), turn out to be equivalent for the tail of the distribution function. Continuous lines are the linear (golden curves) and quadratic (blue curves) extrapolations to $N_{\rm Rep} \to \infty$ for $F(X, T_1, T_2, \xi, r)$ as a function of X. The data shown correspond to the case $T_1 = 0.7$, $T_2 = 0.8$, $\xi = 11$ and $r = 8$. The two curves shown for each extrapolation correspond to the central value plus or minus the standard error. We show horizontal error bars because we are computing the inverse distribution function $X(F, T_1, T_2, \xi, r)$. We only show extrapolated data when $\chi^2/\text{d.o.f} < 1.1$ in the fits to Eq. S1 or to Eq. S2. For comparison, we also plot the data corresponding to $N_{\rm Rep} = 512$ and $N_{\rm Rep} = 256$. *Inset:* As in the main plot, but with the vertical axis in log scale.

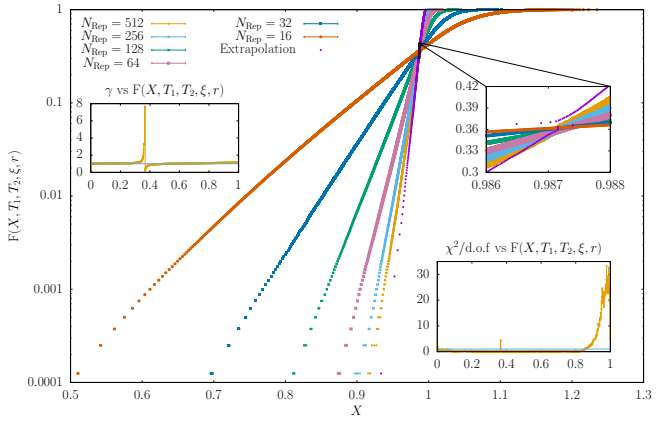

FIG. S2. The exponent γ in Eq. (S3), remains close to one when it becomes a fit parameter. The distribution function $F(X, T_1, T_2, \xi, r)$ is plotted as a function of X for $N_{\rm Rep} = \{512, 256, 128, 64, 32, 16\}$ together with the extrapolation to $N_{\rm Rep} \to \infty$, as obtained from a fit to Eq. (S3). The data shown correspond to $T_1 = 0.7$, $T_2 = 0.8$, $\xi = 11$ and $r = 8$. In order not to clutter the figure, we do not show error bars, that represent one standard deviation, in the $N_{\rm Rep} \to \infty$ extrapolation. *Left inset:* Exponent γ plotted against the probability F. The exponent remains close to $\gamma = 1$ for all F, with the exception of the unstable behavior at $F \approx 0.35$, where curves for different $N_{\rm Rep}$ cross (see also *top-right inset*). *Bottom-right inset:* Goodness-of-fit estimator χ^2 per degree of freedom plotted against F. The blue line corresponds to $\chi^2/\text{d.o.f} = 1$. *Top-right inset:* Closeup of the main plot, emphasizing the crossing region at $F \approx 0.35$. Note that at that particular value of F the data shows almost no dependence with $N_{\rm Rep}$, which makes the fit to Eq. (S3) unstable.

bility in the crossing region around $F \approx 0.35$, see Fig. S2.

In summary, the quadratic and the free-exponent extrapolations support our choice of Eq. S1 as the preferred form for the $N_{\rm Rep} \to \infty$ extrapolation.

SUPPLEMENTARY NOTE 2: CHARACTERIZATION OF THE PEAK

The complementary of the chaotic parameter $1 - X$, as a function of the sphere size, has a well-defined peak. Characterizing the peak is fundamental to the analysis because it provides information about the optimal sphere size for the study of temperature chaos and about the strength of the phenomenon.

Let us remark that, at least close to a maximum, any smooth curve is characterized by the position, height and width of the peak. In order to meaningfully compute these three parameters from our data, we fit $1 - X$ to Eq. (S4) with $z = N_r^{1/3}$. We extract the position, width and height of the maximum from the fitted function $f(z)$. Errors are computed with a jackknife method [1].

SUPPLEMENTARY NOTE 3: ON THE MOST CONVENIENT VARIABLE TO CHARACTERIZE THE SPHERE SIZE

In this section we explain our rationale for choosing the cubic root of the number of spins contained in the sphere, $N_r^{1/3}$, rather than its radius r, to characterize the size of the spheres considered in our analysis.

The objective is fitting the peaks of $1-X$ to a function of the form

$$f(z) = \frac{a z^b}{1 + c z^d}\,, \tag{S4}$$

with a, b, c, and d as fit parameters. If one uses the obvious choice of $z = r$, however, the fit fails. Indeed, see Fig. S3 upper panel, $1 - X$ is not a smooth function of r. The reason is that the number of lattice points in the spheres is not a smooth function of r either (see Fig. S3 lower panel). It is natural, therefore, to replace r with $N_r^{1/3}$ as independent variable. This substitution makes Eq. (S4) work down to smaller spheres. The difference between both independent variables becomes negligible for very large spheres.

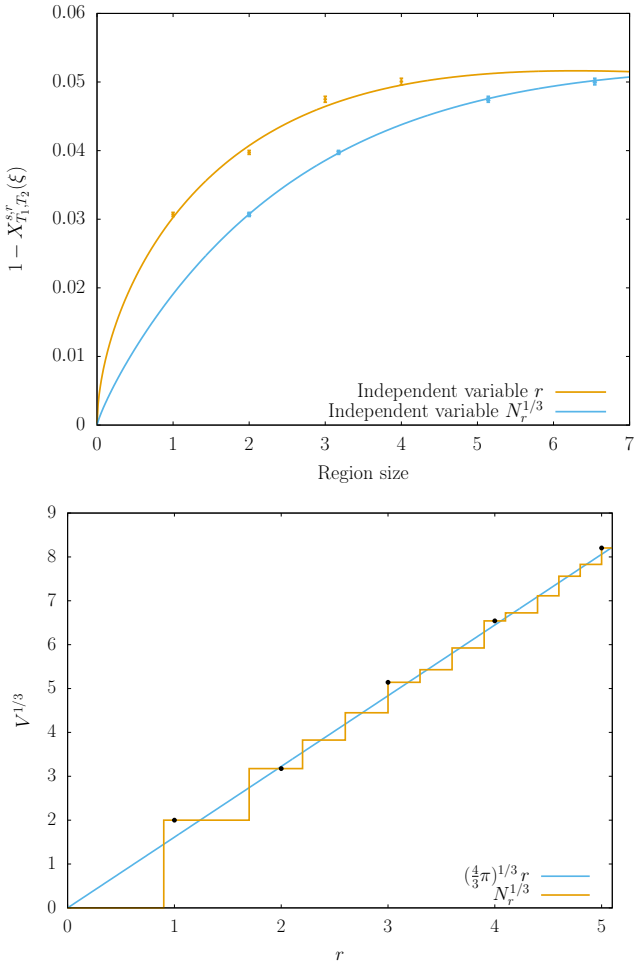

FIG. S3. $N_r^{1/3}$ is a better variable to describe short length scales. *Upper panel:* complementary of temperature chaos $1 - X^{s,r}_{T_1,T_2}(\xi)$ against the region size for the two discussed independent variables, namely $N_r^{1/3}$ and the radius r. The continuous lines are fits to Eq. (S4) taking as variable either $z = r$ (golden curve) or $z = N_r^{1/3}$ (blue curve). The shown data corresponds to $T_1 = 0.7$, $T_2 = 0.9$, $F = 0.01$ and $\xi = 7$. We enlarge the small-sphere region, where both independent variables most differ. Error bars represent one standard deviation. *Lower panel:* the cubic root of the volume of a sphere (blue curve) is plotted as a function of the radius of the sphere r. The golden curve is $N_r^{1/3}$, namely the cubic root of the number of lattice points contained in a sphere of radius r, centered at a node of the dual to our cubic lattice. Values of $N_r^{1/3}$ corresponding to integer r are highlighted as black dots.

SUPPLEMENTARY NOTE 4: GLOBAL VERSUS LOCAL DESCRIPTION OF THE PEAKS

In the main text, we reduce the study of the scaling of temperature chaos with the coherence length ξ to the study of the peak of $1-X$ against the size of the spheres. The reader may wonder whether the local fit of the peak will extend to describe the full curve. Here we present some positive evidences in this respect.

F	T_1	T_2	$\xi_{\min}$	a	b	χ^2/d.o.f
0.001	0.625	0.7	4.75	0.60(12)	0.9(9)	22.12/19
0.001	0.625	0.8	4.75	0.81(7)	0.0(5)	11.52/19
0.001	0.625	0.9	4.75	0.93(10)	0.1(6)	5.35/19
0.001	0.625	1.0	4.75	1.13(13)	−0.6(8)	3.99/19
0.001	0.7	0.8	5.00	0.88(9)	−0.6(7)	38.18/27
0.001	0.7	0.9	4.75	0.98(8)	−0.1(6)	14.90/28
0.001	0.7	0.0	4.75	1.08(7)	−0.2(6)	22.32/28
0.010	0.625	0.8	4.75	1.29(5)	−0.2(3)	22.30/19
0.010	0.625	0.9	4.75	1.47(6)	−0.5(4)	7.32/19
0.010	0.625	1.0	4.75	1.65(6)	−0.8(4)	4.83/19
0.010	0.7	0.8	5.25	1.23(7)	0.2(5)	34.14/26
0.010	0.7	0.9	4.75	1.48(9)	−0.7(6)	17.19/28
0.010	0.7	1.0	4.75	1.63(9)	−0.8(6)	10.81/28

TABLE S1. Parameters obtained in fits of our data for $N^{1/3}_{r,\max}$ to Eq. (S6). For each fit, we also report the figure of merit χ^2/d.o.f (we include in the fit data with $\xi \geq \xi_{\min}$; $\xi_{\min}$ is set by requiring the fit's P value to be larger than 0.05).

Consider any smooth, positive function $H(z)$, with a local maximum at $z = z_{\max}$. Close to this peak, Taylor's theorem implies some (trivial) universality

$$\frac{H(z)}{H(z_{\max})} = 1 - \frac{1}{2} y^2 + \mathcal{O}(y^3)\,, \tag{S5}$$

where $y = \sqrt{\frac{|H''(z_{\max})|}{H(z_{\max})}}(z - z_{\max})$. Note that the peak's position is $z_{\max}$, its heigth is $H(z_{\max})$ and its (inverse) width is $\sqrt{|H''(z_{\max})|/H(z_{\max})}$. In principle, there is no reason for Eq. (S5) to be accurate away from the peak, but this formula suggests an alternative representation for our $1-X$ curves, see Fig. S4. We note that, in this new representation, the $1-X$ curves are invariant under changes of the coherence length ξ (upper panel). When considering changes in the temperatures T_1 and T_2 and the probability F, however, the curves mildly differ away from the peak (see Fig. S4 lower panel). This (approximate) independence of (T_1, T_2, F, ξ) is a fortunate fact because the complexity of the problem gets reduced to the study of the scaling with ξ of the three peak parameters while keeping (T_1, T_2, F) constant.

SUPPLEMENTARY NOTE 5: POSITION AND WIDTH OF THE PEAKS

In this section we analyze the scaling of the peaks' position and width with the coherence length ξ.

We first focus on the peak's position, which signals the most convenient length scale for studying TC (for a given coherence length ξ, probability F and temperatures T_1 and T_2). Dimensional analysis suggests a linear fit as the natural ansatz to study the scaling of the peak's position $N^{1/3}_{r,\max}$ with the coherence length $\xi(t_{\rm w})$ (indeed, both quantities are lengths):

$$N^{1/3}_{r,\max} = a\,\xi(t_{\rm w}) + b\,. \tag{S6}$$

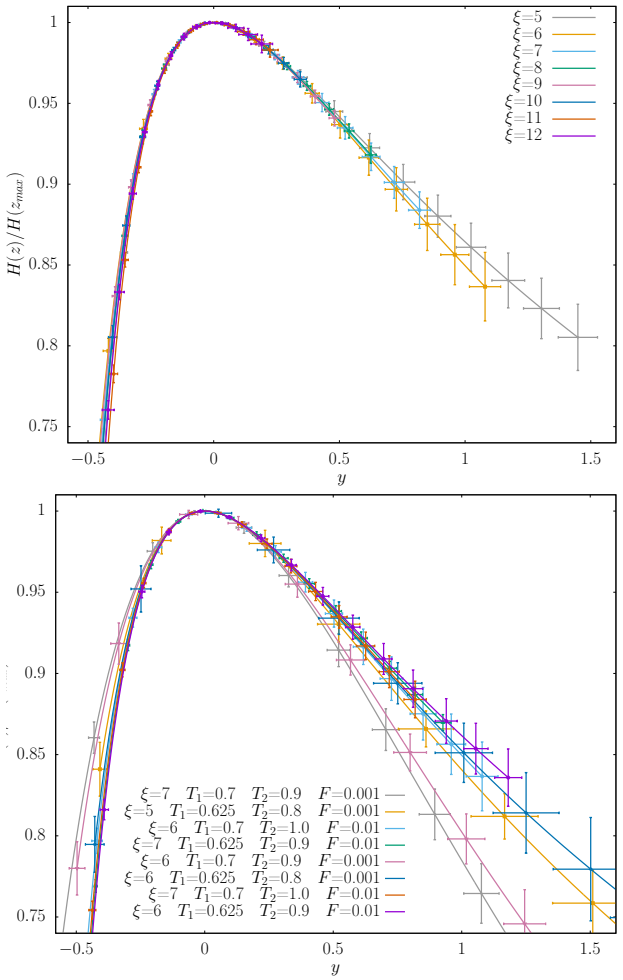

FIG. S4. Universality in $1-X$ extends beyond the trivial Taylor's universality. The upper panel shows $1-X$ in units of its peak value, for the temperatures $T_1 = 0.7$, $T_2 = 1.0$ and $F = 0.01$. Taylor's theorem implies that, using the independent variable y [see Eq. (S5)], the different curves should coincide close to $y = 0$. However, we see that the collapse holds beyond the quadratic approximation (as evinced by the strong asymmetry of the master curve). The lower panel mixes different values of F, T_1 and T_2, which leads to significant discrepancies for large values of $|y|$. Nevertheless, the curves still collapse in a range $y \in (-0.3, 0.5)$ where the asymmetry is significative. Error bars represent one standard deviation.

Fits of the data to Eq. S6 are shown in Table S1. In all cases, values of parameter b are compatible with 0 (at the two-σ level). In addition, amplitude a exhibits monotonic behavior with $T_2 - T_1$ and with the probability F. Hence, our naive expectation $N_{r,\max}^{1/3} \propto \xi(t_w)$ is confirmed.

The peak's width determines how delicate the selection of the right length scale is to study TC (i.e., if the peak's width becomes larger than its position, this choice is no longer critical).

We study the inverse peak's width (i.e., the curvature $\kappa(\xi)$) and propose a power law decaying with $\xi(t_w)$ characterized by the ansatz

$$\kappa(\xi) = A(F)\, \xi^{-\beta}. \tag{S7}$$

F	T_1	T_2	ξmin	A	β	χ^2/d.o.f
0.001	0.625	0.7	4.75	0.8(3)	0.9(2)	18.72/19
0.001	0.625	0.8	4.75	1.6(4)	1.27(14)	8.07/19
0.001	0.625	0.9	4.75	1.4(3)	1.32(12)	10.05/19
0.001	0.625	1.0	4.75	1.3(2)	1.37(9)	5.60/19
0.001	0.7	0.8	4.75	1.1(3)	1.10(12)	35.26/28
0.001	0.7	0.9	4.75	1.26(16)	1.25(7)	25.90/28
0.001	0.7	1.0	4.75	1.19(17)	1.29(7)	23.01/28
0.01	0.625	0.8	4.75	0.63(9)	1.11(7)	20.44/19
0.01	0.625	0.9	4.75	0.59(10)	1.14(8)	6.08/19
0.01	0.625	1.0	4.75	0.58(15)	1.21(12)	9.05/19
0.01	0.7	0.8	4.75	0.59(11)	1.05(12)	21.26/28
0.01	0.7	0.9	4.75	0.63(8)	1.15(7)	18.46/28
0.01	0.7	1.0	4.75	0.59(12)	1.18(9)	17.93/28

TABLE S2. Parameters obtained in fits of our data for $\kappa(\xi)$ to Eq. (S7). For each fit, we also report the figure of merit χ^2/d.o.f (we include in the fit data with $\xi \geq \xi_{\min}$; $\xi_{\min}$ is set by requiring the fit's P value to be larger than 0.05).

Results are shown in Table S2.

The value of $A(F)$ turns out to be compatible for all pairs of temperatures (T_1, T_2) at fixed probability F. Furthermore, at the current precision of the data, exponent β does not exhibit any significant dependence either on the temperature pair (T_1, T_2) or on the probability F.

Let us now recall the linear relation between the peak's position and the coherence length, see Eq. (S6). Consider the ratio between the position of the maximum and its width, $N_{r,\max}\kappa(\xi) \sim \xi^{1-\beta}$. Table S2 mildly suggest that β is slightly greater than 1, which implies that the ratio goes to zero (very slowly) in the limit of large ξ.

[1] F. Belletti, A. Cruz, L. A. Fernandez, A. Gordillo-Guerrero, M. Guidetti, A. Maiorano, F. Mantovani, E. Marinari, V. Martín-Mayor, J. Monforte, A. Muñoz Sudupe, D. Navarro, G. Parisi, S. Perez-Gaviro, J. J. Ruiz-Lorenzo, S. F. Schifano, D. Sciretti, A. Tarancon, R. Tripiccione, and D. Yllanes (Janus Collaboration), J. Stat. Phys. **135**, 1121 (2009), arXiv:0811.2864.